Nanoscale

Targeting myeloid regulators by paclitaxel-loaded enzymatically degradable nanocups

Journal:	*Nanoscale*
Manuscript ID	NR-ART-05-2018-004437.R2
Article Type:	Paper
Date Submitted by the Author:	10-Sep-2018
Complete List of Authors:	Burkert, Seth C.; University of Pittsburgh, Department of Chemistry Shurin, Galina; University of Pittsburgh Medical Center, Department of Pathology White, David ; University of Pittsburgh, Department of Chemistry He, Xiaoyun; University of Pittsburgh, Department of Chemistry Kapralov, Alexander; University of Pittsburgh, Department of Environmental and Occupational Health Kagan, Valerian E.; University of Pittsburgh, Department of Environmental and Occupational Health Shurin, Michael; University of Pittsburgh Medical Center, Department of Pathology Star, Alexander; University of Pittsburgh, Department of Chemistry

SCHOLARONE™
Manuscripts

Please do not adjust margins

Journal Name

ARTICLE

Targeting myeloid regulators by paclitaxel-loaded enzymatically degradable nanocups

Received 00th January 20xx,
Accepted 00th January 20xx

DOI: 10.1039/x0xx00000x

www.rsc.org/

Seth C. Burkert,[a] Galina V. Shurin,[b] David L. White,[a] Xiaoyun He,[a] Alexandr A. Kapralov,[c] Valerian E. Kagan,[a,c,d,e,f] Michael R. Shurin,[b,g], and Alexander Star*[a]

Tumor microenvironment is characterized by immunosuppressive mechanisms associated with the accumulation of immune regulatory cells - myeloid-derived suppressor cells (MDSC). Therapeutic depletion of MDSC has been associated with inhibition of tumor growth and therefore represents an attractive approach to cancer immunotherapy. MDSC in cancer are characterized by enhanced enzymatic capacity to generate reactive oxygen and nitrogen species (RONS) which have been shown to effectively degrade carbonaceous materials. We prepared enzymatically openable nitrogen-doped carbon nanotube cups (NCNC) corked with gold nanoparticles and loaded with paclitaxel as a therapeutic cargo. Loading and release of paclitaxel was confirmed through electron microscopy, Raman spectroscopy and LC-MS analysis. Under the assumption that RONS generated by MDSCs can be utilized as a dual targeting and oxidative degradation mechanism for NCNC, here we report that systemic administration of paclitaxel loaded NCNC delivers paclitaxel to circulating and lymphoid tissue MDSC resulting in the inhibition of growth of tumors (B16 melanoma cells inoculated into C57BL/6 mice) *in vivo*. Tumor growth inhibition was associated with decreased MDSC accumulation quantified by flow cytometry that correlated with bio-distribution of gold-corked NCNC resolved by ICP-MS detection of residual gold in mouse tissue. Thus, we developed a novel immunotherapeutic approach based on unique nanodelivery vehicles, which can be loaded with therapeutic agents that are released specifically in MDSC via NCNC selective enzymatic "opening" affecting change in the tumor microenvironment.

Introduction

Cancer is the second leading cause of death in developed countries with over 12 million new cases diagnosed annually worldwide and the expected number of people suffering from cancer reaching 25 million annually in the next two decades.[1] Nanocarriers are emerging as a valuable tool set in delivering therapeutics in experimental and clinical oncology. Several types of nanocarriers based primarily on liposomes and polymer-protein conjugates have already been approved for clinical use.[2] Recent innovations in nanoscience and nanotechnology are driving novel nanocarriers to clinical translation. Carbon nanotubes are ideal vehicles for this purpose because of the potential for chemical functionalization, proven ability to penetrate mammalian cells and transport biological macromolecules including peptides, proteins, and nucleic acids, and tunable lengths (up to several microns) that can be tailored for cell or organelle penetration.[3-5] However, specialized nanomaterials for precision targeting of the immunosuppressive tumor environment have been difficult to achieve due to the heterogeneous nature of tumors.[6, 7]

Recent research studies have highlighted the important role of myeloid-derived suppressor cells (MDSC), a heterogeneous population of immature myeloid cells, in regulating the antitumor immune response and tumor progression. MDSC are produced in bone marrow and released into the bloodstream where they eventually accumulate in the tumor and lymphoid organs. MDSC accumulate in tumor-bearing hosts and consist of two populations: polymorphonuclear cells (PMN-MDSC) and monocytic cells (M-MDSC).[8, 9] Both of these cell populations have potent immune suppressive activity and have been implicated in promotion of tumor angiogenesis, tumor cell invasion, and metastasis.[10] Tumor-associated MDSC, unlike normal immature myeloid cells, lose the ability to differentiate into conventional dendritic cells (cDC),[11] acquire the ability to differentiate into

[a] *Department of Chemistry, University of Pittsburgh, Pittsburgh, Pennsylvania 15260, United States*
[b] *Department of Pathology, University of Pittsburgh Medical Center, Pittsburgh, Pennsylvania 15261, United States*
[c] *Department of Environmental and Occupational Health, University of Pittsburgh, Pittsburgh, Pennsylvania, United States*
[d] *Department of Pharmacology and Chemical Biology, University of Pittsburgh, Pittsburgh, Pennsylvania, United States*
[e] *Department of Radiation Oncology, University of Pittsburgh, Pittsburgh, Pennsylvania, United States*
[f] *Laboratory of Navigational Redox Lipidomics, IM Sechenov Moscow State Medical University, Russia*
[g] *Department of Immunology, University of Pittsburgh Medical Center, Pittsburgh, Pennsylvania 15261, United States*

† Electronic Supplementary Information (ESI) available: TEM, Raman, and XPS characterization of Au-NCNC from different corking solutions and table of biodistribution of gold as determined by ICP-MS. See DOI: 10.1039/x0xx00000x

This journal is © The Royal Society of Chemistry 20xx

Please do not adjust margins

immunosuppressive regulatory DC,[12] induce differentiation of tolerogenic regulatory T cells (Tregs),[13, 14] support polarization of macrophages into protumorogenic type 2 cells (M2),[15] and suppress activity of innate immune cells like NK cells.[16, 17] Targeting MDSC with certain chemotherapeutic agents, e.g., gemcitabine, cisplatin, and 5-fluorouracil, to induce apoptotic death is a generally accepted therapeutic approach.[18-21] Two potential strategies are differentiation of circulating and lymphoid tissue MDSC prior to accumulation in the tumor microenvironment or direct differentiation of the tumor associated MDSC.[22] The method of targeting circulating and lymphoid tissue MDSC has been overlooked in most traditional therapies. Delivery of high-concentrations of chemotherapeutic agents has typically been correlated with toxicity, hypersensitivity reactions, and neuropathy.[23, 24] We have previously demonstrated that low doses of paclitaxel can down-regulate accumulation and function of MDSC in melanoma and up-regulate their differentiation into immune stimulatory DC.[25, 26] However, clinical applicability of cytotoxic drugs for depleting immune regulators is limited by cumulative toxicity, non-specific effects, immunosuppression and possible pro-metastatic activity.[27-29] Thus, novel approaches for controlled delivery and release of chemotherapeutic agents is highly desirable.

Activated MDSC are characterized by an unusually robust co-expression of NADPH oxidase, ARG-1, iNOS, and myeloperoxidase (MPO) creating an exceptionally potent source of pro-oxidants. NADPH oxidase (particularly NOX2) catalyzed production of superoxide, combined with high levels of $NO^{\bullet}$ production can yield peroxynitrite ($ONOO^{-}$). Dismutation of superoxide creates H_2O_2, a source of oxidizing equivalents for MPO, which facilitates generation of hypochlorous acid (HOCl). These RONS, byproducts of the combined activity of iNOS, MPO, and NOX2, in addition to suppressing activity and longevity of different subsets of immune cells in the tumor milieu,[30] have been shown as effective biodegradation mechanisms of carbonaceous nanoparticles.[31, 32] This arsenal of $ONOO^{-}$ and HOCl-producing enzymatic machineries, uniquely characteristic of MDSC, by far exceeds the capacities of macrophages or neutrophils in generating $ONOO^{-}$ or HOCl, respectively, as carbonaceous nanoparticle biodegradation reagents.

We have previously shown that nitrogen-doped carbon nanotube cups (NCNC) can be separated into individual and short stacked segments, loaded with cargo, corked with gold nanoparticles (Au-NCNC) through sodium citrate reduction of chloroauric acid and subsequently uncorked by potent oxidants enzymatically generated in biochemical models or in inflammatory cells.[33] When Au-NCNC were loaded with paclitaxel and delivered to activated MDSC, immunosuppressive activity of the cells was diminished. Au-NCNC have a length scale greater than 200 nm and are not expected to penetrate the tumor microenvironment as they are too large to be up-taken through the enhanced permeability and retention (EPR) effect.[34] However, due to the overexpression of oxidative biodegradation reagents in MDSC, we expect Au-NCNC to selectively degrade in circulating and lymphoid tissue MDSC resulting in local delivery of paclitaxel and subsequent MDSC differentiation. Here, we report that *in vivo* systemic nanodelivery of Au-NCNC containing paclitaxel inhibited melanoma growth in mice with 25-30% of treated mice being tumor free after 2-3 weeks. ICP-MS tracking of gold atoms indicates that the Au-NCNC do not localize in the tumor mass but instead are found in the spleen and liver resulting in a decrease of MDSC as confirmed by flow cytometry. The results of this investigation provide the proof of concept that systemic targeting of MDSC results in anti-tumor effects without specific targeting to the tumor microenvironment.

Experimental

Synthesis of Au-NCNC

Nitrogen-doped carbon nanotube cups (NCNC) were synthesized through chemical vapor deposition (CVD) synthesis as previously reported.[35] NCNC were then oxidized with mineral acids and separated by probe-tip sonication.[33] Briefly, 10 mg of NCNC were suspended in 40 mL of a 3:1 (v/v) solution of H_2SO_4:HNO_3 and agitated in a bath sonicator for 8 hours at room temperature. The resulting oxidized NCNC were filtered through a 200 nm PTFE membrane and resuspended in nanopure water. The oxidized NCNC in water were then sonicated for 4 hours with a probe-tip ultrasonicator (Qsonica Q500) equipped with a ½ in. probe. The resulting separated NCNC were used for loading and corking reactions. NCNC were corked through a sodium citrate reduction of chloroauric acid similar to our previously published work.[33] NCNC were suspended in 2 mL of 1X phosphate buffer at a concentration around 0.01 mg/mL and stirred on a hot plate at 75°C. A solution of paclitaxel was made in ethanol at a concentration of 2 mg/mL. To load paclitaxel into the NCNC before corking with gold nanoparticles, 50 µL of the paclitaxel solution was added to the NCNC and allowed to stir for 20 minutes. When corking in the absence of paclitaxel, 50 µL of ethanol was added to the empty NCNC for consistency between samples. Next, 100 µL of $HAuCl_4$ aqueous solution (1 mg/mL) was added to the NCNC solution and allowed to stir for 20 minutes. After incubation, 60 µL of 1 wt% trisodium citrate solution was added dropwise and the reaction was stirred for 2 h. Au-NCNC were collected by centrifugation at 1300 x g for 30 min. The resulting supernatant and subsequent washes of the corking solution were analyzed by LC-MS to determine the amount of paclitaxel remaining in the solution.

Material Characterization

TEM images were taken on a FEI Morgagni microscope with an accelerating voltage of 80 kV. High resolution TEM images were taken on a JEOL 2100F microscope with 200 kV accelerating voltage. Samples were drop-cast on lacey carbon TEM grids. Raman spectra were collected from an XplorA Raman AFM-TERS system with a 638 nm (24 mW) laser at 10% laser intensity and 10 s exposure time. XPS characterization was performed on a Thermo ESCALAB 250 Xi XPS using monochromated Al Kα X-rays as the source. DLS and zeta

This journal is © The Royal Society of Chemistry 20xx

potential measurements were performed on a Malvern ZS90 Zetasizer.

MPO degradation of Au-NCNC and paclitaxel quantification by LC-MS

Paclitaxel loaded Au-NCNC were suspended in 446 µL of PBS and 50 µL of water, additions of 2 µL of 2.5 g/L MPO every 6 hours and 2 µL of 25 mM H_2O_2 every hour with 12 additions a day. The samples were incubated at 37°C for 48 hours. The resulting solutions were centrifuged at 1300 x g for 30 mins with the supernatant (top 400 µL) being taken and the paclitaxel collected by dichloromethane (DCM) extraction. After the DCM extraction, the solvent was evaporated and the resulting residue was resuspended in 500 µL of methanol for injection into the LC-MS column. For quantification analysis, 20 µL of 0.5 mg/mL docetaxel was added as an internal standard.

Liquid chromatography was performed using a Dionex-Ultimate 3000 (Thermo Fisher Scientific). The column employed was a Luna-C18(2), 100 x 2.0 mm length and 3 µm particle size from Phenomenex. The mobile phases used were 0.1 % formic acid in water (A) and 0.1 % formic acid in acetonitrile (B). An isocratic program with 50 % A and 50 % B was used. The flow rate was held constant at 200 µL/min with an injection volume of 5 µL.

The LC effluent was pumped into a Q-Exactive benchtop Orbitrap-based mass spectrometer (Thermo Fisher Scientific) with electrospray ionization (ESI) held at a positive polarity. Nitrogen sheath gas and auxiliary gas flow rate were set up at 35 and 10 (arbitrary units), respectively. The capillary temperature was set at 250 °C, spray voltage was 3.5 kV and S-lens voltage set to 60 V. The instrument was operated in targeted single ion monitoring (t-SIM) by selecting the targeted compound (m/z, 854, $M+H]^+$ for paclitaxel) and the internal standard (m/z 808, $[M+H]^+$ for docetaxel) at 70,000 resolving power and the AGC target was $1x10^6$.

Measurements of MPO activity and peroxynitrite production by MDSC

Detection of MPO-activity and peroxynitrite generation was performed using aminophenyl-fluorescein (APF) and hydroxyl-phenyl fluorescein (HPF), respectively. MDSC obtained from normal and B16 melanoma bearing mice were suspended in RPMI 1640 media without phenol red, seeded in a 24-well plate ($150×10^3$ cells/well in a volume of 400 µL), and incubated in the presence of 5 µM APF or 5 µM HPF for 30 min. Activation of cells was performed by addition of 40 nM of PMA. Cell suspensions were analyzed by flow cytometry (FACSanto, BD Biosciences, San Jose, CA).

Animals

6 – 8 week old male C57BL/6 mice were obtained from Taconic. All animals were housed under the standard controlled conditions, and food and water were available *at libitum*. All animal experiments were approved by the Institutional Animal Care and Use Committee and performed in accordance with the Animal Welfare Act and the federal Public Health Service Policy on the Humane Care and Use of Laboratory Animals.

Cell cultures

Murine B16 melanoma cell line (American Type Culture Collection) was maintained in a complete RPMI 1640 medium (GIBCO BRL) supplemented with non-essential amino acids, 10% heat-inactivated fetal bovine serum (FBS), 2 mM L-glutamine, 100 IU/mL penicillin, and 100 µg/mL streptomycin. All tumor cell line cultures were mycoplasma free.

Animal tumor models and experimental designs

B16 cells ($5x10^4$ in 100 µL of saline) were inoculated s.c. in a flank of syngeneic C57BL/6 mice on Day 0. Six days later, tumor-bearing mice were injected i.v. with (i) saline (300 µL, control), (ii) control empty Au-NCNC, (iii) paclitaxel loaded Au-NCNC (300 µL/mouse), and (iv) free paclitaxel (80 µg/mouse). The administered free paclitaxel dosage was determined by taking our maximum delivered dosage from paclitaxel loaded Au-NCNC plus an additional 20%. Paclitaxel was purchased from Mayne Pharma. The tumor size was detected twice per week and expressed as the tumor area (mm^2). All studies included 5-7 mice per group and were independently repeated 2 or 3 times.

For MDSC analysis, tumor tissues were dispersed using 2% collagenase A and 0.75% DNAse I (Roche Diagnostics, Mannheim, Germany) in RPMI 1640 with 10% FBS at 20°C for 1 h using gentleMACS Dissociator (Milteyi Biotec) according to the manufacturer protocols. Spleens were harvested into 5 mL of complete RPMI 1640 medium in a sterile culture dish, grounded, and cell suspensions were filtered through a 70 µm cell strainer. Red blood cells in the lung and spleen were lysed with lysing buffer (155 mM NH_4Cl in 10 mM Tris-HCl buffer pH 7.5, 25°C) for 3 min. After RBC lysis, cells were washed 2 times with FACS buffer (PBS containing 0.1% BSA and 0.05% sodium azide (Sigma, St. Louis, MO)). Cell suspensions were labelled with anti-Ly6G, anti-Ly6C, anti-GR-1 and anti-CD45 antibodies (Biolegend Inc., San Diego, CA) directly conjugated to FITC, PE or Alexa700. Stained cell suspensions were analyzed by flow cytometry (FACSalibur, BD Biosciences, San Jose, CA). Data on MDSC levels in the tumor, lung and spleen are presented as the percentage of cells gated on CD45+ cells.

Detection of gold atoms *in vivo*

Tissue samples were digested based upon a previously published procedure.[36] First, tissue samples were snap frozen in liquid nitrogen and freeze-dried overnight in a Labconco Freezone 6 lyophilizer to remove all water. Each tissue sample was then digested to white ash through the addition of 500 µL of 30% hydrogen peroxide at room temperature. The digested white ash was then further dissolved by the addition of 500 µL of HNO_3. The samples were allowed to sit for 2 days to allow for complete digestion. The samples were then diluted by the addition of 500 µL of nanopure water. In order to dissolve the residual gold from the tissue samples several drops of an *aqua regia* solution, 3:1 hydrochloric acid (Sigma-Aldrich, >99.999 %

trace metal basis): nitric acid (Sigma-Aldrich, >99.99 % trace metal basis), was added to each digested sample and allowed to sit overnight. The resulting solution was filtered through a 200 nm polyvinvylidene fluoride (PVDF) syringe filter to remove any undigested tissue.

Inductively-coupled plasma mass spectrometry (ICP-MS) analysis was performed using an argon flow with a NexION spectrometer (PerkinElmer, Inc.). An *aqua regia* solution was prepared and diluted with water for a 5% (by volume) *aqua regia* matrix. Unknown Au concentrations were determined by comparison to a 5-point standard curve with a range of 1 – 30 ppb (1, 5, 10, 20, and 30 ppb prepared by volume) from a gold standard for ICP (Fluka, TraceCERT 1,001 ± 2 mg/L Au in HCl) diluted in the 5% *aqua regia* matrix. All standards were measured 5 times and averaged, while the unknown samples were measured in triplicate and averaged. A 5 minute flush time with a 5% *aqua regia* matrix was used between all runs, and a blank was analyzed before each unknown sample to confirm removal of all residual metals from the instrument.

Statistical analysis

For a standard comparison of two groups, the Student *t*-test was used after evaluation of normality. If data distribution was not normal, a Mann Whitney rank sum test was performed. For the comparison of multiple groups, analysis of variance was applied. SigmaStat Software was used for the data analysis (SyStat Software, Inc.). For all statistical analyses, $p<0.05$ was considered significant. All experiments were repeated at least two times. Data are presented as the mean ± SEM. Average length and width of Au-NCNC were determined by TEM from 140 measurements and reported as the mean ± standard deviation. DLS size distribution was determined from an average of 3 measurements and reported as the mean ± standard deviation. Zeta potential was determined from an average of 9 measurements and reported as the mean ± standard deviation. LC-MS quantification of paclitaxel loading was performed from 6 individual trials with the average being reported ± the standard deviation.

Results & discussion

The principles of synthesis for Au-NCNC are illustrated in Fig. 1a. Briefly, NCNC were synthesized through a liquid injection chemical vapor deposition (CVD) method and subsequently separated through oxidation with mineral acids followed by probe-tip ultrasonication as previously reported.[37] The resulting separated NCNC were effectively corked with gold nanoparticles through a sodium citrate reduction with $HAuCl_4$.[33, 38] As we have shown previously, the gold nanoparticles preferentially attach to the open end of the separated NCNC due to strong attraction to the dangling amine groups produced through intense probe-tip ultrasonication.[33]

For *in vivo* application of Au-NCNC, alterations to the corking procedure were made to produce sterile Au-NCNC. In order to mimic the biological environment Au-NCNC will be opened under; corking reactions were performed in 2 mL of 1X phosphate buffer (PBS). Corking the NCNC in PBS, as opposed to the normal corking procedure in nanopure water, should also mitigate changes in local biological ion concentrations. Additionally, 50 µL of ethanol was added to the corking

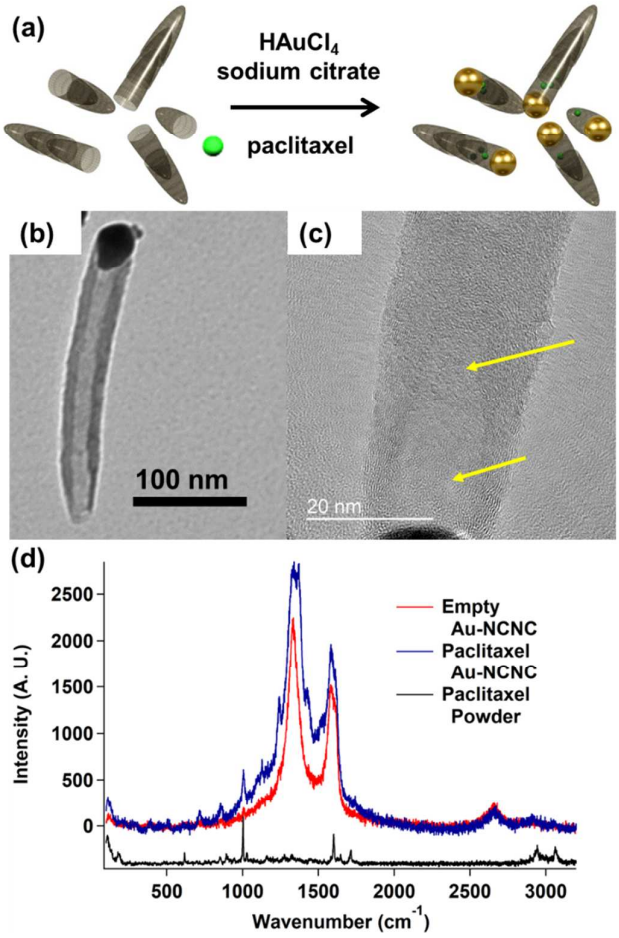

reactions to sterilize the Au-NCNC from biological contaminants and to enhance solubility of hydrophobic paclitaxel in the aqueous corking environment. We believe that the loading of NCNC with paclitaxel is due to hydrophobic interactions between the interior of the cup and the paclitaxel molecule via

Fig. 1 (a) Principles of synthesis for the loading and corking of Au-NCNC; see detailed description in the experimental section. (b) A representative transmission electron microscopy (TEM) image of Au-NCNC. (c) High resolution TEM image illustrating the presence of paclitaxel inside the Au-NCNC; the presence of paclitaxel is highlighted with yellow arrows. (d) Raman spectra of empty Au-NCNC, paclitaxel loaded Au-NCNC, and paclitaxel powder.

a nanoprecipitation reaction facilitated by the evaporation of ethanol from the aqueous corking environment. Nanoprecipitation has previously been reported as an effective technique for loading cisplatin into analogous single-walled carbon nanohorns.[39] The hypothesized strength of the hydrophobic interaction is further confirmed by delivery results (*vide infra*).

A representative TEM image of the final Au-NCNC is shown in Fig. 1b. As can be seen the gold nanoparticle forms a seal

This journal is © The Royal Society of Chemistry 20xx

around the open end of the NCNC. Loading of paclitaxel into the hollow inner cavity of NCNC is illustrated by high resolution TEM (Fig. 1c). Dark areas in the central cavity are observed lacking discernible crystallinity indicating they are not due to the structure of the NCNC. Finally, paclitaxel loading was confirmed by Raman spectroscopy. Gold nanoparticles enhance the Raman signatures of NCNC and the loaded paclitaxel through surface enhancement effects as demonstrated in the Raman spectra of the NCNC under low laser intensity (Fig. 1d).

Changes in the chemical and physical properties of Au-NCNC were monitored due to modifications in the corking procedure for *in vivo* delivery of paclitaxel. We investigated the physical structure of Au-NCNC prepared in (i) nanopure water, (ii) buffer, (iii) buffer and ethanol, and finally (iv) buffer, ethanol, and paclitaxel corking conditions (Fig. S1). TEM revealed no significant differences in the physical structure of Au-NCNC due to the altered corking conditions. However, when ethanol is added to the corking solution, both alone (Fig. S1c) or in combination with paclitaxel (Fig. S1d), free gold nanoparticle formation increased as compared to nanopure water and buffer corking conditions. Despite the increase in free gold nanoparticle formation, a similar percentage (30-40%) of NCNC were found to be completely corked.

The chemical structure of the Au-NCNC did not vary significantly under the several modified corking conditions. Raman spectra shown in Fig. S2 illustrate similar enhancement in the defect peak (D peak, ~1320 cm^{-1}) and graphitic peak (G peak, ~1560 cm^{-1}) of the NCNC, which is due to the presence of the gold nanoparticles in each of the Au-NCNC samples. In addition, nearly identical D/G ratios were detected. Similar Raman intensities confirm that coordination of the NCNC with gold nanoparticles is roughly equivalent. The comparable D/G ratios indicate that changes in the corking conditions do not result in additional defects being incurred by the NCNC structure. Furthermore, survey XPS characteristics do not show any substantial changes in elemental composition of NCNC as illustrated in Fig. S3 and Table S1. The resulting paclitaxel loaded Au-NCNC have an average length of 550 nm ± 260 nm and average width of 55 nm ± 17 nm as measured by TEM. Length distribution was confirmed with DLS measurements with an average size of 513 nm ± 21 nm. Furthermore, the zeta potential of the paclitaxel loaded Au-NCNC was found to be – 39.9 mV ± 1.9 mV in nanopure water at a pH of 6 indicating colloidally stable particles as shown in Fig S4.

Liquid chromatography and mass spectrometry (LC-MS) was utilized to track paclitaxel for two goals: 1) establish that paclitaxel is loaded within the interior of Au-NCNCs and is released upon incubation with MPO/H_2O_2/Cl^- and 2) determine the amount of the loaded paclitaxel. Successful observation of paclitaxel by LC-MS enabled quantification through comparing to an internal standard, docetaxel, and creating a calibration curve of the area ratios between the two molecules.[40] LC-MS chromatograms of both paclitaxel and docetaxel can be seen in Fig. S5. A calibration curve for quantifying paclitaxel in the μg/mL range was constructed as observed in Fig. S6. The supernatant of the corking solution after centrifugation and the resulting washes were analyzed by LC-MS to determine the amount of paclitaxel remaining in solution after the corking reaction. The initial corking solution had 100 μg of paclitaxel and the remaining supernatant and washing solutions had 64 μg ± 23 μg. Therefore, the amount of loaded paclitaxel to the interior of Au-NCNC is 36 μg ± 23 μg resulting in a roughly 36% loading efficiency which correlates with our previously reported corking efficiency based on TEM.[33]

Paclitaxel loaded Au-NCNC were incubated with MPO and H_2O_2 in PBS buffer for 0, 24, and 48 hours. Upon completion of the MPO uncorking of the paclitaxel loaded Au-NCNC, the solution was centrifuged and the supernatant collected for paclitaxel extraction. DCM extraction was performed to collect any released paclitaxel resulting from uncorking. As a control, an empty Au-NCNC sample was also incubated with MPO and H_2O_2 for 48 hours with the same extraction performed. The amount of paclitaxel in these samples was quantified through LC-MS and the constructed calibration curve as seen in Table 1. At 0 hours, the area ratio of the paclitaxel is low enough that it can be assumed no paclitaxel is present. After 24 and 48 hours of incubation with MPO and H_2O_2 paclitaxel begins to be released from the cups as the released mass of paclitaxel in the solution is 0.302 μg and 0.910 μg respectively as shown in Table 1. The empty control sample does not show any paclitaxel indicating that no by-products of the MPO oxidation of Au-NCNC interfere with the paclitaxel quantification. These results demonstrate that paclitaxel is released slowly over time as only 3% of the loaded paclitaxel has been released after 48 hours of incubation with MPO. The hydrophobic interaction of paclitaxel with the interior of the NCNC is strong enough to require complete degradation of the NCNC for total release of paclitaxel despite the uncorking of gold occurring after 24 hours. We hypothesize that this strong interaction promotes a slow delivery of the therapeutic agent.

Table 1. Quantified amount of paclitaxel upon uncorking Au-NCNC

Sample	**Area Ratio**	**Taxol Release** (μg)
0 hour	0.010	–
24 hours	0.088	0.302
48 hours	0.265	0.910
48 hours control	0.009	–

The release of paclitaxel is also correlated to the uncorking of the Au-NCNC as observed by TEM and Raman spectroscopy shown in Fig. 2. In Fig. 2a, Au-NCNC were incubated with MDSC for 48 hours before being collected. The gold nanoparticle corks are removed from the NCNC where the inset TEM image shows a gold nanoparticle which is only partly associated to the opening of the NCNC. In Fig. 2b, Au-NCNC were incubated with MPO, H_2O_2, and NaCl for 0, 24, and 48 hours before being collected and Raman spectra measured. As MPO incubation proceeds the gold nanoparticles are removed from the NCNC, as evidenced by TEM images, thus lowering the Raman enhancement due to the association of the plasmonic particles with the graphitic structure. For

comparison a Raman spectrum of separated NCNC without any attached gold nanoparticles is also presented.

Our delivery mechanism for the uncorking of Au-NCNC is *via* an incubation with MPO and/or other enzymatic pathways providing RONS and chlorinating products as we have previously illustrated *in vitro*.[33, 41] We expect MDSC from tumor-bearing mice to be highly effective in opening and degrading Au-NCNC due to high levels of expression of MPO, NADPH oxidase, and iNOS. In fact, tumor-activated MDSC from tumor-bearing animals exert a higher level of MPO and $ONOO^-$ generating

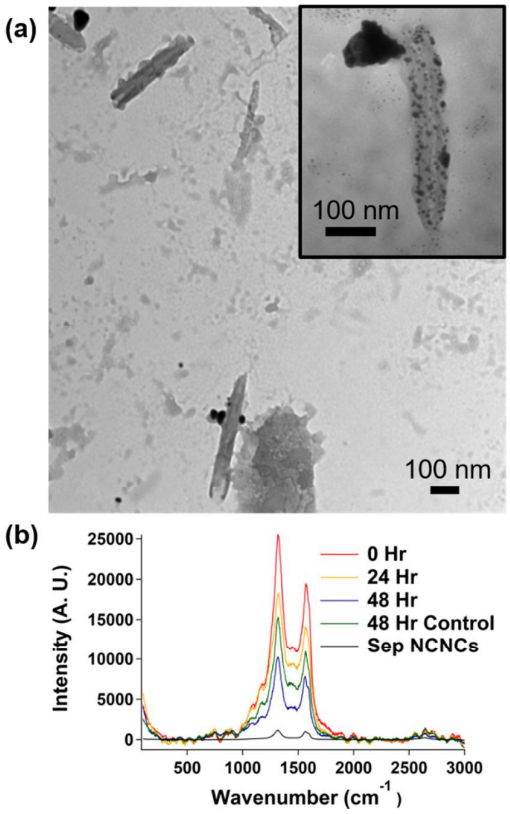

Fig. 2 (a) TEM images illustrating the uncorking and degradation of Au-NCNC upon incubation with MDSC. (b) Raman spectroscopy illustrating the uncorking of Au-NCNC upon incubation with MPO, H_2O_2, and NaCl in comparison to pristine NCNC.

activity than non-activated MDSC from control tumor-free mice as illustrated in Fig. 3a. In these experiments, we used aminophenyl-fluorescein (APF) as a substrate for MPO and hydroxyl-phenyl fluorescein (HPF) for assessments of peroxynitrite-driven oxidants.[42, 43] In both cases, highly fluorescent products were formed after oxidation reactions driven by MPO or $ONOO^-$, respectively. We observe a ~2 fold higher oxidative potency detectable in the presence of MDSC from tumor-bearing animals compared to control non-activated cells (Fig. 3b, $p<0.05$). The addition of Au-NCNC caused a marked decrease in HPF/APF fluorescence emission intensity ($p<0.05$), indicating that a significant portion of the reactive intermediates was interacting with Au-NCNC rather than with the fluorescent probes. Therefore, MDSC from tumor bearing mice produce larger amounts of oxidizing agents providing an avenue for degradation of the paclitaxel loaded Au-NCNC. The pro-oxidative environment allows the Au-NCNC to be selectively degraded within MDSC minimizing the need for targeting ligands.

To determine whether paclitaxel-loaded Au-NCNC display unique drug delivery characteristics *in vivo*, we assessed tumor (melanoma) growth in syngeneic animals treated with saline, empty Au-NCNC, Au-NCNC loaded with paclitaxel, and free paclitaxel as described above. We have previously shown that systemic delivery of 1-5 mg/kg doses of paclitaxel in different tumor models can restore immune function *in vivo*.[26] However, the effect was observed only after multiple injections or in

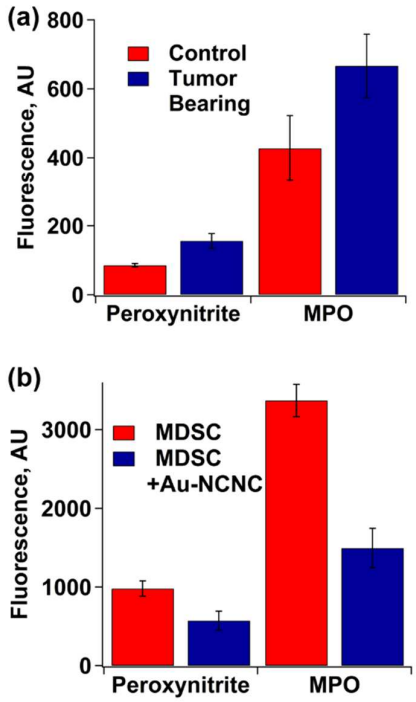

This journal is © The Royal Society of Chemistry 20xx

Fig. 3 (a) MPO activity and peroxynitrite ($ONOO^-$) production in MDSC isolated from tumor-free (control, red) and tumor-bearing (blue) mice were assessed as described in materials and methods. (b) Activated MDSC can target Au-NCNC as reflected by decreased activity of MPO and expression of $ONOO^-$ after addition of NCNC (blue) as compared to control MDSC (red). Au-NCNC are oxidized by PMA-activated MDSC resulting in the decrease in the MPO and $ONOO^-$ responses.

combination with other therapies. As the loaded amount of paclitaxel was found to be on average 36 µg, the total administered dosage of paclitaxel was 1.8 mg/kg. We administered one injection of the paclitaxel loaded Au-NCNC per mouse and measured the therapeutic effect over 3 weeks. Time-course of tumor growth in all groups of melanoma-bearing mice is shown in Fig. 4. Control mice without Au-NCNC injection have a linear/exponential increase in tumor size over the course of more than two weeks, as expected. Injection of empty Au-NCNC results in a slight decrease in the rate of tumor growth, which can be attributed to non-specific inflammation associated with systemic nanomaterial administration. Immune cells are characterized by the expression of oxidative enzymes and the expression of these enzymes increases in response to pro-inflammatory conditions.[44, 45] More specifically, the introduction of nanomaterials to biological systems has been shown to trigger such a pro-inflammatory response. Incubation of macrophages with MWCNTs was found to induce activity of COX-2 and iNOS which are responsible for the metabolism of arachidonic acid into prostaglandins and production of NO respectively which are both central to inflammatory response.[46] Shortening CNTs has typically been seen as a way to decrease these effects; however the incorporation of structural and chemical defects after specific shortening techniques have been correlated with enhanced pro-inflammatory and pro-oxidative responses.[47] Therefore, the marginal decrease in tumor growth

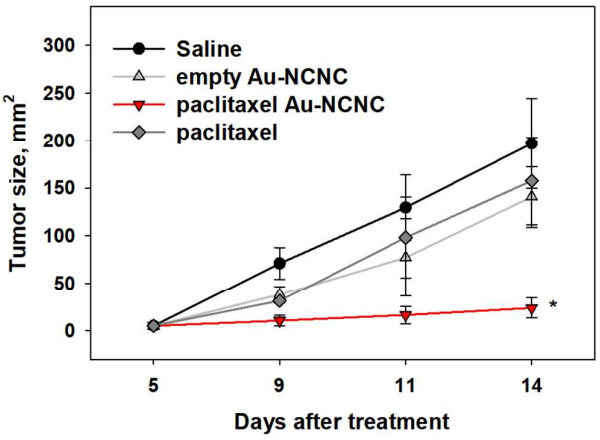

Fig. 4 B16 melanoma cells were inoculated s.c. in syngeneic mice on day 0 and on day 6 animals were treated with saline (control), empty Au-NCNC, paclitaxel loaded Au-NCNC, and free paclitaxel. Tumor growth was measured as described in the experimental section. The results are shown as Mean ± SEM. *, $p < 0.01$ (ANOVA, n = 3 experiments).

in response to empty Au-NCNC is most likely due to the activation of these pro-inflammatory machineries. Treatment with paclitaxel-loaded Au-NCNC results in significant inhibition of tumor growth in melanoma-bearing mice ($p<0.05$, n=3). The effect observed is more pronounced as compared to empty Au-NCNC indicating that the anti-tumor effect is not due to non-specific inflammation and must be due to the delivery of paclitaxel. Furthermore, ~25-30% of mice injected with paclitaxel-loaded Au-NCNC were found to be tumor-free on day 15. A single administration of free paclitaxel in tumor bearing mice did not significantly alter tumor growth. This confirms our early studies showing noncytotoxic doses of this chemotherapeutic agent (less than 20 – 30 mg/kg as a single injection) do not display a significant antitumor potential in the B16 melanoma model.[48-50] Thus, Au-NCNC based delivery of paclitaxel, unlike free paclitaxel results in significant inhibition of tumor growth *in vivo*. Injection of free paclitaxel affects a slight decrease in tumor growth between days 5 and 9. Decreased tumor growth was short-lived as growth rates returned to similar values as the saline injection for the remainder of the *in vivo* trial. In comparison, delivery of paclitaxel by Au-NCNC resulted in prolonged effects over the entire time course of the *in vivo* experiment. This further illustrates a strong interaction of the paclitaxel with the interior cavity of the NCNC resulting in gradual release of the loaded cargo as opposed to a burst delivery of chemotherapeutic agent.

While bio-distribution of paclitaxel has been previously studied through LC-MS, these experiments were performed at time points less than 24 hours.[51, 52] Therefore, the gold nanoparticle corks, which act to effectively seal the NCNC openings, also provide a unique label for tracking the distribution of Au-NCNC upon *in vivo* delivery. Gold atom concentrations were tracked through digestion of mouse tissue followed by quantification by inductively coupled plasma mass
spectrometry (ICP-MS). To determine homing and distribution of gold atoms in mice *in vivo*, heart, lung, liver, spleen, and tumor tissue were collected from treated animals at different time points. The tissue samples were then digested based upon previously published procedure.[36] Gold concentrations in each tissue sample were evaluated at days 6, 8 and 13 after injection
of paclitaxel loaded and empty Au-NCNC. Comparisons between the biodistribution of empty Au-NCNC and paclitaxel loaded NCNC are not desirable due to the ability of paclitaxel to alter maturation and thus phagocytic activity and homing of myeloid phagocytes like macrophages, DC, MDSC, and neutrophils. In fact, paclitaxel is a known inhibitor of neutrophil function and longevity.[53] We have previously reported that paclitaxel could stimulate maturation of DC, alter their endocytic activity and change DC motility.[54-56]

Others have shown that nanodelivered paclitaxel changed the phagocytic properties of liver macrophages.[57] Therefore, we focus on the bio-distribution of gold in response to i.v. injection of paclitaxel loaded Au-NCNC as shown in Fig. 5.

The initial bio-distribution of paclitaxel loaded Au-NCNC as determined by ICP-MS shows the most accumulation of gold within the liver, followed by the spleen and negligible accumulation within the heart and tumor. While long-term comparisons between empty and paclitaxel loaded Au-NCNC are undesirable, due to differences in phagocytic activity in response to delivered paclitaxel, initial bio-distribution of gold in response to i.v. injection of empty Au-NCNC was found to be similar to paclitaxel loaded Au-NCNC as shown in Table S2. The bio-distribution of gold after i.v. injection of paclitaxel loaded Au-NCNC are highlighted in Fig. 5 indicating a decrease in the amount of gold located within the liver while a simultaneous increase in the amount of gold located within the spleen over time. The temporal change in distribution can be attributed to the difference in bio-distribution between gold nanoparticles and carbon nanotubes. Previous reports have shown that introduction of carbon nanotubes *in vivo* results in an initial accumulation within the liver.[58] Similar studies on the bio-distribution of gold nanoparticles found that the particles mainly accumulate in the spleen upon *in vivo* exposure.[36] We believe that the initial spike of gold atoms in the liver is due to gold nanoparticles still being associated with NCNC and therefore following the normal bio-distribution of the carbon nanotube. After several days, the gold nanoparticles have been detached from the nanotube surface by oxidation and proceed on their normal bio-distribution thus accumulating in the spleen. The amount of gold found within the heart is plotted as a control as gold nanoparticles are not expected to reside within heart tissue for extended periods of time. ICP-MS analysis of gold bio-distribution also indicates that the gold does not reside within the tumor for extended periods of time. This illustrates that due to the length scale of Au-NCNC, they are not up-taken by the tumor microenvironment and therefore delivery of paclitaxel directly to the tumor is not expected. Instead, Au-NCNC are up-taken by circulating and lymphoid tissue MDSC where they are uncorked and paclitaxel is locally delivered. This represents a novel chemotherapeutic technique altering circulating and lymphoid tissue MDSC instead of targeting the tumor microenvironment. The complete ICP-MS data including gold bio-distribution of empty Au-NCNC are summarized in Table S2.

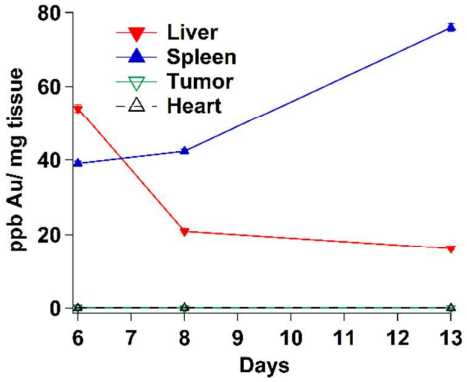

Fig. 5 Inductively coupled plasma mass spectrometry (ICP-MS) was used to detect gold atoms in different tissues 6, 8, and 13 days after i.v. injection of paclitaxel loaded Au-NCNC as described in experimental techniques. The results were normalized per milligram of tissue. Each sample was run in triplicate with the average being reported and error bars representing the standard deviation of the triplicate measurements.

Monitoring the levels of MDSC subsets in both lymphoid and non-lymphoid tissues across the time course of the experiment, by flow cytometry, was used to evaluate whether the antitumor activity of paclitaxel loaded Au-NCNC *in vivo* is associated with down-regulation of MDSC and potential correlation with gold distribution. Fig. 6 (upper panels) shows that administration of paclitaxel loaded Au-NCNC was accompanied by a rapid and prolonged decrease of the percentage of intratumoral PMN-MDSC up to 4-5 fold ($p<0.05$, $n=2$). Interestingly, no significant alterations of intratumoral M-MDSC were seen after Au-NCNC administration, which may be due to the differential sensitivity of intratumoral MDSC subsets to paclitaxel. We have recently reported that PMN-MDSC but not M-MDSC in the tumor milieu may differentiate in regDC and that paclitaxel might affect this pathway of myeloid regulatory cell interdifferentiation.[12]

We conducted a similar evaluation of both MDSC subsets in dynamics after intravenous injection of empty and paclitaxel loaded Au-NCNC in the spleen and lungs, the organs known for high tropism and homing of MDSC. Tumor-bearing mice receiving either saline or free paclitaxel served as controls. It is important to notice that the level of MDSC was determined within CD45+ cells, i.e. leukocytes: also known as leukocyte common antigen, CD45 is expressed on almost all hematopoietic cells except for mature erythrocytes.[59] This fact is documented by low levels of MDSC in the spleen, which are enriched with leukocytes. The results of these studies (Fig. 6 and S7) confirm that the treatment of melanoma-bearing mice with paclitaxel loaded Au-NCNC is accompanied by a decrease in MDSC in different lymphoid and non-lymphoid tissues, in conjunction with a decrease in the tumor mass. However, injection of free paclitaxel does not have the same effect as MDSC levels were found to be similar to those of mice injected with saline (Fig. S7). These data agree with our results suggesting that corked NCNC might be opened in different tissues where myeloid regulatory cells, in particular MDSC, are expected to be accumulated during tumor growth and progression. Furthermore, both monocytic and polymorphonuclear MDSC were affected by NCNC delivered

This journal is © The Royal Society of Chemistry 20xx

paclitaxel confirming the fact that in tumor-bearing hosts MDSC infiltrating the tumor bed are functionally different from MDSC homing in other tissues, including spleen, lymph nodes, bone marrow and non-lymphoid organs. Finally, no vital signs of toxicity or autoimmune processes in mice receiving i.v. Au-NCNC were observed up to 40 – 50 days after nanomaterial administration. Together, these results strongly support the feasibility of using Au-NCNC loaded with anti-cancer agents in diseases where marked accumulation and/or activation of myeloid regulatory cells is anticipated.

Delivery of paclitaxel to the tumor microenvironment has been attempted with prodrug nanoparticles and liposomes; however these drug delivery systems rely on external stimuli for delivery either through the form of external irradiation or induced hyperthermia.[60, 61] Additionally, polymeric nanoparticles have illustrated the ability to exploit reactive oxygen species as a stimuli for drug delivery.[62, 63] Our unique nano-delivery material is characterized by two major advantages over analogous drug delivery vehicles; first, our results do not require specific functionalization for targeting the tumor microenvironment simplifying our production process, and second our enzymatic opening mechanism is specific for the unique MDSC oxidizing environment resulting in minimal non-specific delivery without any externally provided stimulus. Additionally, our drug delivery system does not need to be combined with additional therapies to halt tumor progression unlike analogous materials,[61] and does not require the use of paclitaxel derivatives and can instead use the unmodified molecule.[64]

Conclusions

We have demonstrated the usefulness of Au-NCNC for the delivery of paclitaxel in the context of cancer immunotherapy. Altering the gold nanoparticle corking mechanism for *in vivo* applications had minimal effect on the physical and chemical properties of Au-NCNC. Upon intravenous injection Au-NCNC were found to distribute throughout the body and not specifically in the tumor microenvironment. Despite non-exclusive targeted delivery, paclitaxel was released from Au-NCNC and presumably affected the local populations of MDSC. Our results provide proof of concept for not only the use of Au-NCNC as a unique immunotherapy but that targeting circulating and lymphoid tissue MDSC can result in a pronounced antitumor effect without specifically targeting the tumor microenvironment. Based on our earlier *in vitro* data showing that paclitaxel released from Au-NCNC in the presence of tumor-activated MDSC did not induce apoptosis of MDSC but augmented MDSC differentiation into cDc,[33] we speculate that the similar mechanism may also operate *in vivo*. Knowing the wide spectrum of immunomodulating properties of paclitaxel,[65] additional antitumor pathways induced by enzymatically degraded paclitaxel loaded corked NCNC can be suggested.

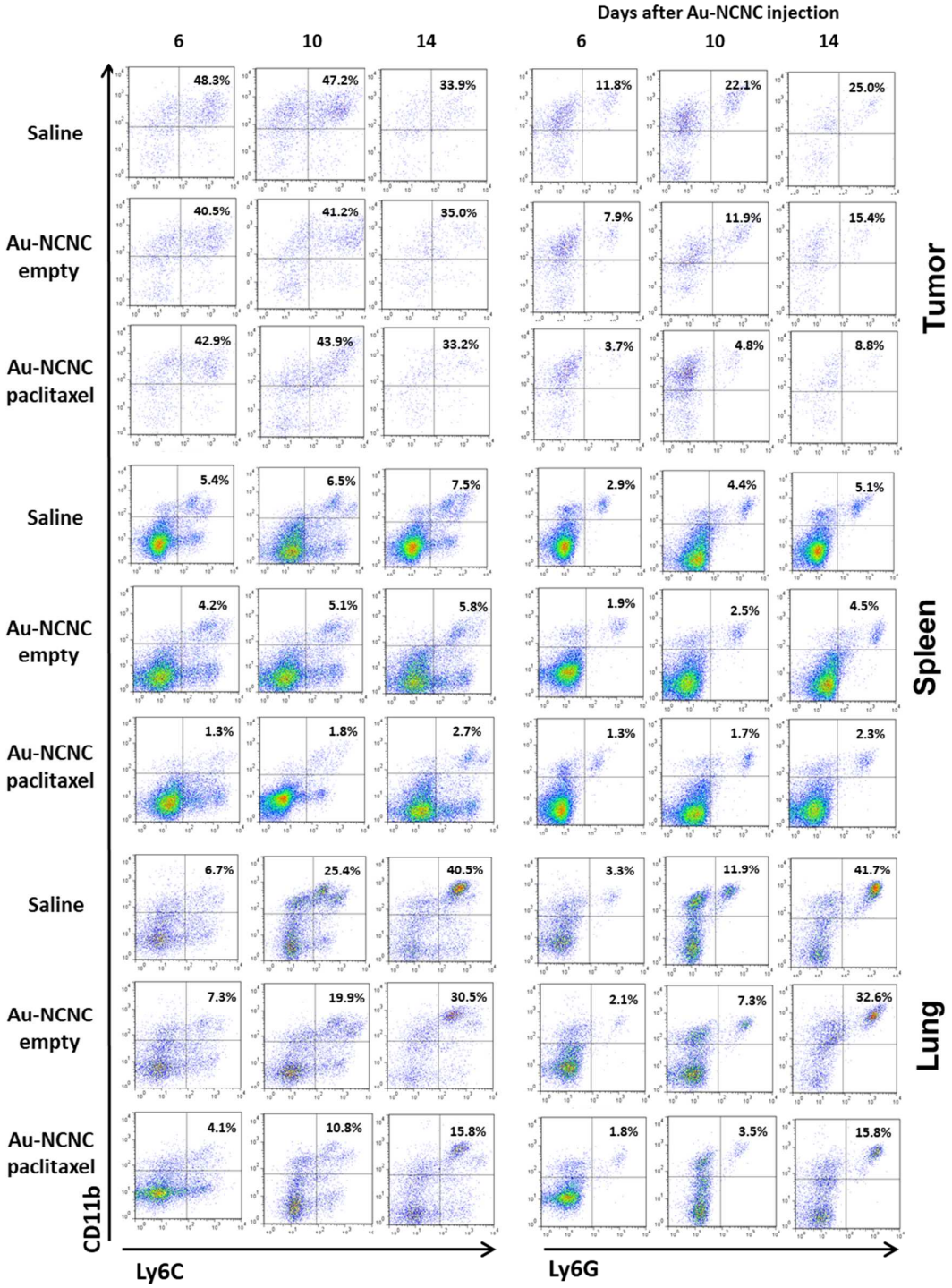

Fig. 6 B16 melanoma-bearing mice were i.v. injected with saline, empty Au-NCNC and paclitaxel loaded Au-NCNC and tissues were harvested at different time points as shown. Tissues were digested, and single cell suspensions were prepared and stained as described in materials and methods. Representative flow cytometry results are shown for CD45 gated cell populations. The levels of monocytic CD11bLy6C^{high}Ly6G$^{low/neg}$ M-MDSC and polymorphonuclear CD11bLy6G^{high}Ly6C$^{low/neg}$ PMN-MDSC are shown. Two independent experiments revealed similar results.

Their evaluation, as well as systemic characterization of antitumor potential of Au-NCNC loaded with different

This journal is © The Royal Society of Chemistry 20xx

chemotherapeutic, targeted and immunotherapeutic compounds in different pre-clinical tumor models is timely and well justified.

Conflicts of interest

There are no conflicts to declare.

Acknowledgements

This work at the University of Pittsburgh was supported by an NSF CAREER Award No. 0954345, NIH R01ES019304, and NIH R01CA154369. Raman characterization was completed through the assistance of a ONR (N000141410765) grant. We thank the Nanoscale Fabrication and Characterization Facility and the Department of Biological Sciences at the University of Pittsburgh for provision of access to the TEM and Raman instruments. Special thanks to Ashley Smith, Kathryn Johnston, and Daniel J. Bain for use and operation of the ICP-MS. Special thanks to Dr. Bhaskar Godugu for assistance with LC-MS method development.

Notes and references

1. K. Saika and T. Sobue, *Gan to kagaku ryoho Cancer & chemotherapy*, 2013, **40**, 2475-2480.
2. D. Peer, J. M. Karp, S. Hong, O. C. Farokhzad, R. Margalit and R. Langer, *Nat. Nanotechnol.*, 2007, **2**, 751-760.
3. S. W. Kim, T. Kim, Y. S. Kim, H. S. Choi, H. J. Lim, S. J. Yang and C. R. Park, *Carbon*, 2012, **50**, 3-33.
4. K. Kostarelos, L. Lacerda, G. Pastorin, W. Wu, S. Wieckowski, J. Luangsivilay, S. Godefroy, D. Pantarotto, J.-P. Briand, S. Muller, M. Prato and A. Bianco, *Nat. Nanotechnol.*, 2007, **2**, 108-113.
5. V. Sanna, N. Pala and M. Sechi, *Int. J. Nanomed.*, 2014, **9**, 467-483.
6. M. G. Sikkandhar, A. M. Nedumaran, R. Ravichandar, S. Singh, I. Santhakumar, Z. C. Goh, S. Mishra, G. Archunan, B. Gulyas and P. Padmanabhan, *Int. J. Mol. Sci.*, 2017, **18**, E1036.
7. L. Tan and Y. H. Bae, *Colloids Surf., B*, 2012, **99**, 116-126.
8. D. I. Gabrilovich, *Cancer Immunol. Res.*, 2017, **5**, 3-8.
9. V. Bronte, S. Brandau, S.-H. Chen, M. P. Colombo, A. B. Frey, T. F. Greten, S. Mandruzzato, P. J. Murray, A. Ochoa, S. Ostrand-Rosenberg, P. C. Rodriguez, A. Sica, V. Umansky, R. H. Vonderheide and D. I. Gabrilovich, *Nat. Commun.*, 2016, **7**.
10. J. E. Talmadge and D. I. Gabrilovich, *Nat. Rev. Cancer*, 2013, **13**, 739-752.
11. S. Ostrand-Rosenberg, *BMC Proc.*, 2013, **7(Suppl 2)**, K20.
12. H. Zhong, D. W. Gutkin, B. Han, Y. Ma, A. A. Keskinov, M. R. Shurin and G. V. Shurin, *Int. J. Cancer*, 2014, **134**, 2633-2645.
13. J. Wang, L. Yang, L. Yu, Y.-Y. Wang, R. Chen, J. Qian, Z.-P. Hong and X.-S. Su, *Oncotarget*, 2017, **8**, 17050-17058.
14. B. Huang, P.-Y. Pan, Q. Li, A. I. Sato, D. E. Levy, J. Bromberg, C. M. Divino and S.-H. Chen, *Cancer Res.*, 2006, **66**, 1123-1131.
15. P. Sinha, V. K. Clements, S. K. Bunt, S. M. Albelda and S. Ostrand-Rosenberg, *J. Immunol.*, 2007, **179**, 977-983.
16. J. Sceneay, M. T. Chow, A. Chen, H. M. Halse, C. S. F. Wong, D. M. Andrews, E. K. Sloan, B. S. Parker, D. D. Bowtell, M. J. Smyth and A. Moller, *Cancer Res.*, 2012, **72**, 3906-3911.
17. E. Suzuki, V. Kapoor, A. S. Jassar, L. R. Kaiser and S. M. Albelda, *Clin. Cancer Res.*, 2005, **11**, 6713-6721.
18. R. Wesolowski, J. Markowitz and W. E. Carson, *J. Immunother. Cancer*, 2013, **1**, 10.
19. K. H. Parker, D. W. Beury and S. Ostrand-Rosenberg, *Adv. Cancer Res.*, 2015, **128**, 95-139.
20. D. D. Mitri, A. Toso and A. Alimonti, *Clin. Cancer Res.*, 2015, **21**, 1-5.
21. K. N. Kodumudi, K. Woan, D. L. Gilvary, E. Sahakian, S. Wei and J. Y. Djeu, *Clin. Cancer Res.*, 2010, **16**, 4583-4594.
22. V. Kumar, S. Patel, E. Tcganov and D. I. Gabrilovich, *Trends Immunol.*, 2016, **37**, 208-220.
23. V. J. Poirier, A. E. Hershey, K. E. Burgess, B. Phillips, M. M. Turek, L. J. Forrest, L. Beaver and D. M. Vail, *J. Vet. Intern. Med.*, 2004, **18**, 219-222.
24. T. Iwamoto, *Biol. Pharm. Bull.*, 2013, **36**, 715-718.
25. T. Michels, G. V. Shurin, H. Naiditch, A. Sevko, V. Umansky and M. R. Shurin, *J. Immunotoxicol.*, 2012, **9**, 292-300.
26. A. Sevko, T. Michels, M. Vrohlings, L. Umansky, P. Beckhove, M. Kato, G. V. Shurin, M. R. Shurin and V. Umansky, *J. Immunol.*, 2013, **190**, 2464-2471.
27. M. R. Shurin, *Nat. Med.*, 2013, **19**, 20-22.
28. M. R. Shurin, H. Naiditch, D. W. Gutkin, V. Umansky and G. V. Shurin, *Curr. Med. Chem.*, 2012, **19**, 1792-1803.
29. S. Gingis-Velitski, D. Loven, L. Benayoun, M. Munster, R. Bril, T. Voloshin, D. Alishekevitz, F. Bertolini and Y. Shakad, *Cancer Res.*, 2011, **71**, 6986-6996.
30. S. Ugel, F. D. Sanctis, S. Mandruzzato and V. Bronte, *J. Clin. Invest.*, 2015, **125**, 3365-3376.
31. I. I. Vlasova, A. A. Kapralov, Z. P. Michael, S. C. Burkert, M. R. Shurin, A. Star, A. A. Shvedova and V. E. Kagan, *Toxicol. Appl. Pharmacol.*, 2016, **299**, 58-69.
32. K. Bhattacharya, S. P. Mukherjee, A. Gallud, S. C. Burkert, S. Bistarelli, S. Bellucci, M. Bottini, A. Star and B. Fadeel, *Nanomed. - Nanotechnol.*, 2016, **12**, 333-351.
33. Y. Zhao, S. C. Burkert, Y. Tang, D. C. Sorescu, A. A. Kapralov, G. V. Shurin, M. R. Shurin, V. E. Kagan and A. Star, *J. Am. Chem. Soc.*, 2015, **137**, 675-684.
34. H. Maeda, *Adv. Enzyme Regul.*, 2001, **41**, 189-207.
35. Y. Tang, S. C. Burkert, Y. Zhao, W. A. Saidi and A. Star, *J. Phys. Chem. C*, 2013, **117**, 25213-25221.
36. C. Lasagna-Reeves, D. Gonzalez-Romero, M. A. Barria, I. Olmedo, A. Clos, V. M. S. Ramanujam, A. Urayama, L. Vergara, M. J. Kogan and C. Soto, *Biochem. Biophys. Res. Commun.*, 2010, **393**, 649-655.
37. H. Dong, Y. Zhao, Y. Tang, S. C. Burkert and A. Star, *ACS Appl. Mater. Interfaces*, 2015, **7**, 10734-10741.
38. S. C. Burkert and A. Star, *Curr. Protoc. Chem. Biol.*, 2015, **7**, 249-262.
39. K. Ajima, M. Yudasaka, T. Murakami, A. Maigné, K. Shiba and S. Iijima, *Mol. Pharm.*, 2005, **2**, 475-480.
40. C. d. G. Lux, S. Joshi-Barr, T. Nguyen, E. Mahmoud, E. Schopf, N. Fomina and A. Almutairi, *J. Am. Chem. Soc.*, 2012, **134**, 15758-15764.
41. W. Seo, A. A. Kapralov, G. V. Shurin, M. R. Shurin, V. E. Kagan and A. Star, *Nanoscale*, 2015, **7**, 8689-8694.

This journal is © The Royal Society of Chemistry 20xx

42. P. Wardman, *Free Radic. Biol. Med.*, 2007, **43**, 995-1022.
43. J. Flemmig, P. Schwarz, I. Bäcker, A. Leichsenring, F. Lange and J. Arnhold, *J. Immunol. Methods*, 2014, **415**, 46-56.
44. B. Brüne, N. Dehne, N. Grossmann, M. Jung, D. Namgaladze, T. Schmid, A. v. Knethen and A. Weigert, *Antioxid. Redox Signaling*, 2013, **19**, 595-637.
45. H. Mangge, K. Becker, D. Fuchs and J. M. Gostner, *World J. Cardiol.*, 2014, **6**, 462-477.
46. J. K. Lee, B. C. Sayers, K.-S. Chun, H.-C. Lao, J. K. Shipley-Phillips, J. C. Bonner and R. Langenbach, *Part. Fibre Toxicol.*, 2012, **9**, 14.
47. C. Bussy, M. Pinault, J. Cambedouzou, M. J. Landry, P. Jegou, M. Mayne-L'hermite, P. Launois, J. Boczkowski and S. Lanone, *Part. Fibre Toxicol.*, 2012, **9**, 46.
48. H. Zhong, B. Han, I. L. Tourkova, A. Lokshin, A. Rosenbloom, M. R. Shurin and G. V. Shurin, *Clin. Cancer Res.*, 2007, **13**, 5455-5462.
49. H. Naiditch, M. R. Shurin and G. V. Shurin, *Immunol. Res.*, 2011, **50**, 276-285.
50. J. P. Landreneau, M. R. Shurin, M. V. Agassandian, A. A. Keskinov, Y. Ma and G. V. Shurin, *Cancer Microenviron.*, 2015, **8**, 57-64.
51. R. Li, J. S. Eun and M.-K. Lee, *Arch. Pharm. Res.*, 2011, **34**, 331-337.
52. D. Mandal, T. K. Shaw, G. Dey, M. M. Pal, B. Mukherjee, A. K. Bandyopadhyay and M. Mandal, *Int. J. Biol. Macromol.*, 2018, **112**, 818-830.
53. R. L. Roberts, J. Nath, M. M. Friedman and J. I. Gallin, *J. Immunol.*, 1982, **129**, 2134-2141.
54. G. V. Shurin, I. L. Tourkova, R. Kaneno and M. R. Shurin, *J. Immunol.*, 2009, **183**, 137-144.
55. G. V. Shurin, I. L. Tourkova and M. R. Shurin, *J. Immunother.*, 2008, **31**, 491-499.
56. R. Kaneno, G. V. Shurin, I. L. Tourkova and M. R. Shurin, *J. Transl. Med.,* 2009, **7**, 58.
57. T. Tanei, F. Leonard, X. Liu, J. F. Alexander, Y. Saito, M. Ferrari, B. Godin and K. Yokoi, *Cancer Res.*, 2016, **76**, 429-439.
58. Z. Liu, W. Cai, L. He, N. Nakayama, K. Chen, X. Sun, X. Chen and H. Dai, *Nat. Nanotechnol.*, 2007, **2**, 47-52.
59. A. Nakano, T. Harada, S. Morikawa and Y. Kato, *Acta. Pathol. Jpn.*, 1990, **40**, 107-115.
60. Q. Pei, X. Hu, X. Zheng, S. Liu, Y. Li, X. Jing and Z. Xie, *ACS Nano*, 2018, **12**, 1630-1641.
61. Y. Lv, C. Xu, X. Zhao, C. Lin, X. Yang, X. Xin, L. Zhang, C. Qin, X. Han, L. Yang, W. He and L. Yin, *ACS Nano*, 2018, **12**, 1519-1536.
62. Y. Dai, S. Cheng, Z. Wang, R. Zhang, Z. Yang, J. Wang, B. C. Yung, Z. Wang, O. Jacobson, C. Xu, Q. Ni, G. Yu, Z. Zhou and X. Chen, *ACS Nano*, 2018, **12**, 455-463.
63. Y. Wang, Y. Deng, H. Luo, A. Zhu, H. Ke, H. Yang and H. Chen, *ACS Nano*, 2017, **11**, 12134-12144.
64. W. Tang, J. Yang, Y. Yuan, Z. Zhao, Z. Lian and G. Liang, *Nanoscale*, 2017, **9**, 6529-6536.
65. A. Javeed, M. Ashraf, A. Riaz, A. Ghafoor, S. Afzal and M. M. Mukhtar, *Eur. J. Pharm. Sci.*, 2009, **38**, 283-290.

TOC Graphic:

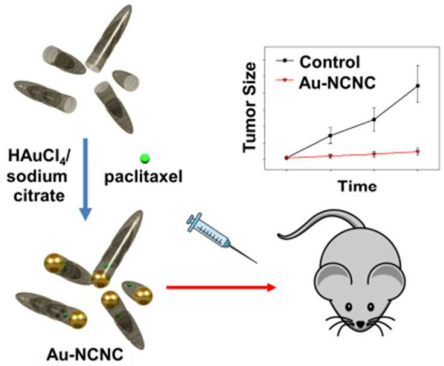

TOC Summary: Carbon nanomaterial assisted delivery of paclitaxel to circulating and lymphoid tissue MDSC as proof of concept immunotherapy strategy *in vivo*.

This journal is © The Royal Society of Chemistry 20xx